arXiv:astro-ph/0306546v1 26 Jun 2003

SPECTRAL ENERGY DISTRIBUTION IN SUPERCRITICAL DISK ACCRETION FLOWS THROUGH PHOTON-TRAPPING EFFECTS

K. Ohsuga, S. Mineshige, and K. Watarai
Yukawa Institute for Theoretical Physics, Kyoto University, Kyoto 606-8502, Japan
Draft version February 2, 2008

ABSTRACT

We investigate the spectral energy distribution (SED) of the supercritical disk accretion flows around black holes by solving the multi-frequency zeroth moment equation of the radiation transfer equation under the flux-limited diffusion approximation as well as the energy equation of gas. Special attention is paid to the photon-trapping effects, the effects that photons are trapped within accretion flow and are swallowed by a black hole, with little being radiated away. It is found that when flow luminosity is below about twice the Eddington luminosity ($L \lesssim 2L_E$) photon trapping is ineffective and the SED shifts to the higher-energy side as L increases. The peak frequency at which the SED reaches its peak becomes at maximum three times higher than that given by the standard-disk model, which might resolve the so-called 'too hot accretion disk problem.' When $L \gtrsim 2L_E$, in contrast the peak frequency of the SED tends to decrease with increase of mass-accretion rate. This is due to enhanced photon-trapping. Since high-energy photons are generated near the equatorial plane, they can be more effectively trapped in flow than low-energy ones and, hence, the high energy part of radiation is suppressed. Finally, the observed time variation of IC 342 S1, which is an ultraluminous X-ray source, in the X-ray HR diagram can be explained by the modulation of the mass accretion rate. In comparison with the observational data, we estimate the mass of black hole in IC 342 S1 is $\sim 100M_\odot$.

Subject headings: accretion: accretion disks — black hole physics — radiative transfer

1. INTRODUCTION

The standard-disk model proposed by Shakura & Sunyaev (1973) has had some success in describing optically thick accretion flow structure in luminous objects, such as X-ray binary sources in the soft state. However, the standard-disk model is constructed under number of approximations and its treatment is only justified when the mass-accretion rate, $\dot{M}$, is less than the critical mass-accretion rate, $\dot{M}_{crit}$, where the critical mass-accretion rate is given by $\dot{M}_{crit} \equiv L_E/c^2$ with the Eddington luminosity, $L_E = 4\pi cGMm_p/\sigma_T$, where c, M, m_p, and σ_T are the light velocity, the black-hole mass, the proton mass, and the Thomson scattering cross-section, respectively. Since the mass-accretion rate is determined by some mechanism which is independent of the nature of the central star itself (Alme & Wilson 1976; Spruit & Ritter 1983; Norman & Scoville 1988; King et al. 1997; Umemura, Fukue, & Mineshige 1998; Ohsuga et al. 1999), there are no reasons why $\dot{M}$ should always be below $\dot{M}_{crit}$. That is, the supercritical accretion flow may naturally arise. Indeed, several possible sites of super- or near-critical accretion flow have been suggested; e.g., micro-quasars (Yamaoka, Ueda, & Inoue 2001), ultraluminous X-ray sources (ULXs) (Okada et al. 1998; Colbert & Mushotzky 1999; Mizuno et al. 1999; Makishima et al. 2000; Watarai et al. 2000; Revnivtsev et al. 2002), narrow-line Seyfert 1 galaxies (Boller 2000; Mineshige et al. 2000), quasars (Collin et al. 2002), and Gamma-ray bursts (Narayan, Piran, & Kumar 2001; Kohri & Mineshige 2002).

When the mass-accretion rate exceeds the critical value, photon trapping plays an important role within the trapping radius,

$$r_{trap} \sim \dot{m} \left(\frac{H}{r} \right) r_g, \tag{1}$$

where $\dot{m}$ is the mass-accretion rate normalized by the critical mass-accretion rate, H is the disk-half thickness, r is the radius, and r_g is the Schwarzschild radius (Ohsuga et al. 2002, hereafter referred to as Paper I, see also Begelman 1978 for the spherical case). Thus, the radiation energy, which is generated by viscosity in the vicinity of the black hole, is trapped in the flow and advected inward without being immediately radiated away. Since the advective energy transport was firstly considered in the slim-disk model by Abramowicz et al. (1988), in the context of the accretion-disk models this model has been believed to be the solution of the supercritical disk accretion flow (Kato, Fukue, & Mineshige 1998). However, it is shown in Paper I that the photon-trapping effects are not accurately treated in the slim-disk approach. The reason for this is that the time delay between the energy generation deep inside the disk and the energy release at the surface is not taken into account in the slim-disk formulation, although the time delay is not negligible and exceeds the accretion timescale within the trapping radius.

In the light of the recent discovery of the supercritically accreting objects, it is of great importance to study the spectral energy distribution (SED) of the supercritical disk accretion flow. But, little is known about the SED of the flow suffering the photon-trapping effects except for the case of the slim-disk model. Szuszkiewicz, Malkan, & Abramowicz (1996) and Watarai et al. (2000) have calculated the SED of the slim disk by superposition of blackbody/modified-blackbody spectra. Wang et al. (1999) have solved the radiation transfer equations in the vertical direction, coupling with the slim-disk formu-

lation. As we noted above, however, the slim-disk model has not fully considered the photon-trapping effects, so we need further studies.

In paper I, we investigated the photon-trapping effects in the disk accretion flow, but only solved the monochromatic radiation transfer equations inside the accretion flow. In this work, we investigate the SED of the optically-thick supercritical accretion flows by solving multi-frequency radiation transfer equations. In §2, we give our model and the basic equations. The resultant SEDs are presented in §3. Comparing our results with the observational data, we discuss the role of the photon trapping in the actual objects. Finally, §4 and §5 are devoted to discussion and conclusions, respectively.

2. OUR MODEL AND BASIC EQUATIONS

In this section, we numerically solve the multi-frequency radiation-transfer equations, as well as the energy equations of gas and radiation, by taking into account the photon-trapping effects. Since we are concerned with the radiation processes, especially the photon-trapping effects themselves, we employ a simple model for the accretion flow structure (see Paper I).

Here, the cylindrical coordinates, (r, φ, z), are used. We consider that the accretion disk is axisymmetric and steady in the Eulerian description; $\partial/\partial\varphi = \partial/\partial t = 0$. We employ the Gaussian density profile in the vertical direction,

$$\rho(r, z) = \rho_0(r) \exp\left[-\left(\frac{z}{H}\right)^2\right], \qquad (2)$$

where ρ_0 is the gas density on the equatorial plane and we assume the ratio of the disk-half thickness to the radius, H/r, to be a constant in radius, depending on $\dot{m}$;

$$\frac{H}{r} = \varepsilon_{100}\left(\frac{\dot{m}}{10^2}\right), \qquad (3)$$

with ε_{100} being a dimensionless parameter representing the aspect ratio, H/r, at $\dot{m} = 100$. Such a linear relation between H/r and $\dot{m}$ exactly holds in the radiation pressure-dominated part of the standard-disk model [see, e.g., equation (3.61) of Kato, Fukue, & Mineshige (1998)], and also roughly holds in the slim-disk model as long as $\dot{m}$ is less than a few hundreds (Watarai et al. 2000). The density on the equatorial plane, ρ_0, is related to the surface density as,

$$\Sigma(r) = 2\rho_0(r)\int_{-\infty}^{\infty}\exp\left[-\left(\frac{z}{H}\right)^2\right]dz = 2\sqrt{\pi}\rho_0(r)H(r), \qquad (4)$$

where the surface density, Σ, is calculated by the continuity equation for a given accretion rate, $\dot{M}$,

$$\dot{M} = -2\pi r v_r \Sigma, \qquad (5)$$

with v_r being the radial component of the velocity.

Since the radial component of the velocity, v_r, is related to the viscosity parameter α through $v_r \sim -\alpha\left(H/r\right)c_s$ with c_s being the sound velocity (see, e.g., Frank, King, & Raine 1985; Kato, Fukue, & Mineshige 1998), and H is given by the equation (3), v_r is finally expressed in terms of the free-fall velocity as

$$v_r = -\alpha\varepsilon_{100}^2\left(\frac{\dot{m}}{10^2}\right)^2\left(\frac{GM}{r}\right)^{1/2}. \qquad (6)$$

The vertical component is prescribed as

$$v_z = \frac{z}{r}v_r, \qquad (7)$$

i.e., we assume a convergence flow.

Through equations (3), (5), and (6), Σ and ρ are related to ε_{100} and $\dot{m}$ in our model; $\Sigma \propto \varepsilon_{100}^{-2}\dot{m}^{-1}$ and $\rho \propto \varepsilon_{100}^{-3}\dot{m}^{-2}$. The photon-trapping radius is rewritten by using equation (3) as,

$$r_{\rm trap} \sim 10^{-2}\varepsilon_{100}\dot{m}^2 r_{\rm g}. \qquad (8)$$

Here, it is noted that the photon-trapping radius not only indicates the critical radius for the photon trapping but also expresses the significance of the photon-trapping effects, since this relation is derived from the comparison between the accretion timescale and the radiative diffusion timescale. Thus, the photon-trapping effects are more pronounced in the case of larger ε_{100} and $\dot{m}$.

We suppose the structure of the accretion disk to be locally plane parallel; that is, the disk is regarded as consisting of accreting ring elements (see discussion in the end of this section). Each ring is composed of N layers in the z-direction, and the thickness of each layer is $\Delta z = 2H_0/N$ (see Figure 2 of Paper I). Here, H_0 defines the upper boundary of the disk in the numerical simulations in such a way that $\rho(r, H_0) = 0.1\rho_0(r)$. We solve the time-dependent energy fields of gas and radiation in the ring element during the course of accretion motion until the element reaches the inner edge of the disk. Both of the viscous heating and compressional heating though converging inflow are considered. Since the flow assumed to be steady ($\partial/\partial t = 0$), time coordinate can be transformed to the spatial coordinates; i.e., $D/Dt = v_r\partial/\partial r + v_z\partial/\partial z$ with v_r and v_z being given by equations (6) and (7). We thus express the multi-frequency radiative flux at the disk surface as a function of radius and then calculate the resultant SED and luminosity of the disk.

In the plane-parallel approximation, the radial and azimuthal components of the radiative flux are null. Also, non-diagonal components of the radiation stress tensor are null. Hence, using equations (6) and (7), we write the energy equations of radiation and gas as

$$\rho\left(v_r\frac{\partial}{\partial r} + \frac{z}{r}v_r\frac{\partial}{\partial z}\right)\left(\frac{E_\nu}{\rho}\right)$$
$$= -\frac{\partial F_\nu^z}{\partial z} - \frac{v_r}{r}\nu\frac{\partial}{\partial\nu}\left(\frac{1}{2}P_\nu^{rr} - P_\nu^{\varphi\varphi} - P_\nu^{zz}\right)$$
$$+ 4\pi\kappa_\nu B_\nu - c\kappa_\nu E_\nu, \qquad (9)$$

and

$$\rho\left(v_r\frac{\partial}{\partial r} + \frac{z}{r}v_r\frac{\partial}{\partial z}\right)\left(\frac{e}{\rho}\right)$$
$$= -\frac{3}{2}\frac{v_r}{r}p_{\rm gas} - 4\pi\kappa_P B + c\kappa_E E + q_{\rm vis}, \qquad (10)$$

respectively, where E_ν and $E(\equiv \int E_\nu d\nu)$ are the radiation energy density and its frequency-integrated form, respectively, F_ν^z is the radiative flux in the z-direction, P_ν^{ii} is the diagonal (ii-th) components of the radiation stress tensor, B_ν and $B = \sigma T_{\rm gas}^4/\pi$ are the Planck function and its frequency-integrated form, respectively, with $T_{\rm gas}$ being the gas temperature and σ being the Stefan-Boltzmann constant, $\kappa_\nu = 3.7\times10^8 T_{\rm gas}^{-1/2}(\rho/m_{\rm p})^2\nu^{-3}\{1-$

$\exp(-h\nu/kT_{\mathrm{gas}})\}$ is the free-free absorption coefficient (Rybicki & Lightman 1979), with h being the Planck constant and k being the Boltzmann constant, e is the internal energy density, p_{gas} is the gas pressure, κ_P and κ_E are the Planck-mean and energy-mean opacities, respectively,

$$\kappa_P = \frac{1}{B}\int \kappa_\nu B_\nu d\nu, \qquad (11)$$

$$\kappa_E = \frac{1}{E}\int \kappa_\nu E_\nu d\nu, \qquad (12)$$

and q_{vis} is the viscous heating rate per unit volume (Mihalas & Klein 1982; Mihalas & Mihalas 1984; Fukue, Kato, & Matsumoto 1985; Stone, Mihalas, & Norman 1992).

To close the set of equations, we apply the multi-frequency flux-limited diffusion approximation (FLD), for the radiative flux and stress tensor,

$$F_\nu^z = -\frac{c\lambda_\nu}{\chi_\nu}\frac{\partial E_\nu}{\partial z}, \qquad (13)$$

$$P_\nu^{rr} = P_\nu^{\varphi\varphi} = \frac{1}{2}(1-f_\nu)E_\nu, \qquad (14)$$

and

$$P_\nu^{zz} = f_\nu E_\nu, \qquad (15)$$

with χ_ν being the extinction coefficient,

$$\chi_\nu = \frac{\rho\sigma_{\mathrm{T}}}{m_{\mathrm{p}}} + \kappa_\nu, \qquad (16)$$

where λ_ν, R_ν, and f_ν are defined as

$$\lambda_\nu = \frac{2+R_\nu}{6+3R_\nu+R_\nu^2}, \qquad (17)$$

$$R_\nu = \frac{1}{\chi_\nu E_\nu}\left|\frac{\partial E_\nu}{\partial z}\right|, \qquad (18)$$

and

$$f_\nu = \lambda_\nu + \lambda_\nu^2 R_\nu^2. \qquad (19)$$

These relations correspond to the multi-frequency form of the monochromatic FLD represented by Turner & Stone (2001). This approximation holds both in the optically thick and thin regimes. In the optically thick limit ($R_\nu \to 0$), we find $\lambda_\nu \to 1/3$ and $f_\nu \to 1/3$. In the optically thin limit of $R_\nu \to \infty$, on the other hand, we have $|F_\nu^z| = cE_\nu$, $P_\nu^{rr} = P_\nu^{\varphi\varphi} = 0$, and $P_\nu^{zz} = E_\nu$. These give correct relations in the optically thick diffusion limit and optically thin streaming limit, respectively. Thus, we can rewrite the radiation energy equation (9) as

$$\rho\left(v_r\frac{\partial}{\partial r} + \frac{z}{r}v_r\frac{\partial}{\partial z}\right)\left(\frac{E_\nu}{\rho}\right)$$
$$= c\frac{\partial}{\partial z}\left(\frac{\lambda_\nu}{\chi_\nu}\frac{\partial E_\nu}{\partial z}\right) + \frac{v_r}{r}\nu\frac{\partial}{\partial\nu}\left(\frac{3f_\nu+1}{4}E_\nu\right)$$
$$+4\pi\kappa_\nu B_\nu - c\kappa_\nu E_\nu. \qquad (20)$$

These nonlinear equations (10) and (20) are integrated iteratively by the Newton-Raphson method with the Gauss-Jordan elimination for a matrix inversion, by being coupled with the equation of state,

$$p_{\mathrm{gas}} = \frac{2}{3}e. \qquad (21)$$

We employ the simple model for viscous heating rate, whose distribution in the z-direction is proportional to the total pressure; that is,

$$q_{\mathrm{vis}}(r,z) = Q_{\mathrm{vis}}(r)\frac{E(r,z)+2e(r,z)/3}{\int_0^{H_0}\{E(r,z)+2e(r,z)/3\}\,dz}, \qquad (22)$$

where Q_{vis} is the half vertically-integrated viscous heating rate per unit surface,

$$Q_{\mathrm{vis}} \sim \frac{3}{8\pi}\Omega_{\mathrm{K}}^2\dot{M}\left[1-\left(\frac{r_{\mathrm{in}}}{r}\right)^{1/2}\right], \qquad (23)$$

(Shakura & Sunyaev 1973; Lynden-Bell & Pringle 1974), with Ω_{K} being the Keplerian angular speed.

Throughout the present study, α and N are set to be 0.1 and 100, respectively. We consider the range of frequency, $\log\nu = 16-20$, with $\Delta\log\nu = 0.08$. Since the radiative flux from the vicinity of the black hole gives negligible contribution to the total SED due to the large redshift in the face-on case, we neglect the emission from the regions inside, $r < 3r_{\mathrm{g}}$ [see, e.g., equation (3.159) of Kato, Fukue, & Mineshige (1998)]. The supercritical disk becomes relatively geometrically thick through the strong radiation pressure and is obscured by the outer part of the disk in the edge-on case so that it would be observed as objects of small inclination angle. The black-hole mass is fixed to be $10M_\odot$ except in §3.4, where we adopt $50M_\odot$ and $100M_\odot$ to compare our results with the observations of ULXs.

In our simulations, we assumed the disk to be locally plane parallel. Hence, the radiation energy diffuses towards only the z-direction in the frame moving with gas; i.e., the radial and azimuthal components of the radiative flux are null. However, if the radial gradient of the radiation energy density is comparable to the vertical one, $|\partial E/\partial z| \sim |\partial E/\partial r|$, the diffusion of the radiation energy towards the r-direction is not negligible. Such a situation would hold in the very vicinity of the inner edge of the disk, where the radiation energy effectively falls onto the black hole because of $F^r < 0$. Thus, the photon trapping would be enhanced at $r \lesssim 3r_{\mathrm{g}}$. In contrast, the radiative flux would become positive, $F^r > 0$, at $r > 3r_{\mathrm{g}}$, and may not be negligible if the aspect ratio, H/r, is of the order of unity. In this case, the photon-trapping effects would be reduced. Such a reduction of the photon trapping is roughly estimated as follows. Since the radiative diffusion timescale is given by c/τ, the ratio of the radial diffusion velocity and vertical diffusion velocity is roughly obtained to be $v_{\mathrm{diff,r}}/v_{\mathrm{diff,z}} \sim \tau_z/\tau_r \sim H/r$. Here, $\tau_z \sim \rho\sigma_{\mathrm{T}}H/m_{\mathrm{p}}$ and $\tau_r \sim \rho\sigma_{\mathrm{T}}r/m_{\mathrm{p}}$ are the optical depth for the Thomson cross-section in vertical and radial directions, respectively. By taking into account the radiative diffusion in the radial direction, the timescale for the radiation energy to be swallowed by the black hole is $\tau_{\mathrm{swa}} \sim r/(v_r - v_{\mathrm{diff,r}})$. By comparison between this timescale and the diffusion timescale in vertical direction, $H/(c/\tau_z)$, we find that the photon-trapping radius is modified as

$$r'_{\mathrm{trap}} \sim r_{\mathrm{trap}}\left\{1+\left(\frac{H}{r}\right)^2\right\}^{-1}, \qquad (24)$$

where equations (1), (5), $\tau_z = \sigma_{\mathrm{T}}\Sigma/m_{\mathrm{p}}$, $\dot{M}_{\mathrm{crit}} \equiv L_{\mathrm{E}}/c^2$, and $L_{\mathrm{E}} = 4\pi cGMm_{\mathrm{p}}/\sigma_{\mathrm{T}}$ are used. Since the luminosity depends on the trapping radius as $L \sim \int_{r_{\mathrm{trap}}} 2\pi r Q_{\mathrm{vis}}dr \propto r_{\mathrm{trap}}^{-1}$ (Paper I), the luminosity would increase by a factor of $1+(H/r)^2$ on account of the radiative diffusion in the radial direction. For $\varepsilon_{100} = 0.5$, our formulation underestimate luminosity by $(H/r)^2 \sim 0.25(\dot{m}/100)^2$. Doppler beaming tends to focus radiation field to be more confined within the equatorial plane, thereby enhancing the photon

trapping effects. The details would be elucidated by solving two-dimensional radiation transfer equations as future work.

3. RESULTS

3.1. *Luminosity*

We first plot the luminosity against the mass-accretion rate in Figure 1, where the luminosity and mass-accretion rate are normalized by the Eddington luminosity and the critical mass-accretion rate, respectively. The luminosity should increase along the dashed line, if the energy-conversion efficiency, $\eta \equiv \dot{M}c^2/L$, is constant. However, it is found that the energy-conversion efficiency decreases with increase in the mass-accretion rate at $L \gtrsim 2L_E$ due to the photon trapping. We also see that the larger ε_{100} is, the lower becomes the luminosity at high mass-accretion rates, $\dot{m} \gg 10$. This can be understood, since the photon-trapping effects are more conspicuous for larger ε_{100} [see equation (8)]. We have confirmed the results of Paper I, whereby energy-conversion efficiency decreases with increase of the mass-accretion rate, by the multi-frequency radiation transfer simulations.
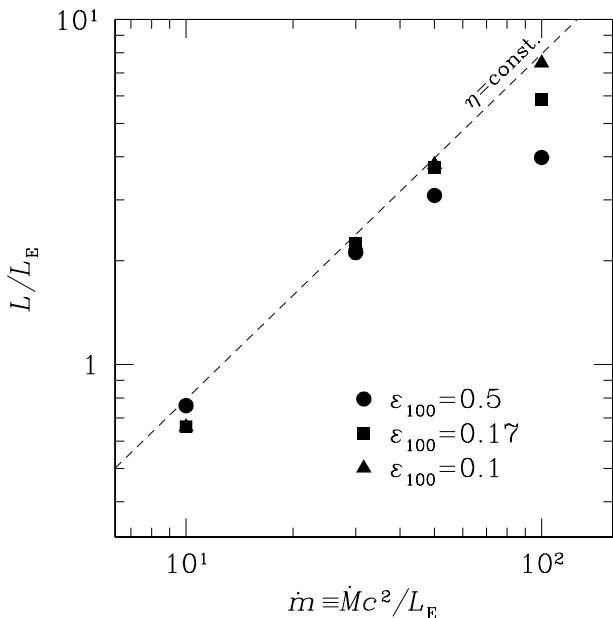

FIG. 1.— Total disk luminosity as a function of the mass-accretion rate, $\dot{m} \equiv \dot{M}c^2/L_E$. The circles, squares, and triangles represent the cases with $\varepsilon_{100} = 0.5$, 0.17, and 0.1, respectively, where ε_{100} is a dimensionless parameter defined as $\varepsilon_{100} \equiv (H/r)/(\dot{m}/100)$. The dashed line shows the luminosity for the cases that the energy-conversion efficiency, $\eta \equiv \dot{M}c^2/L$, is kept constant.

3.2. *Effective Temperature*

The effective temperature profile is shown in Figure 2. Here, the effective temperature is defined as $T_{\rm eff} = (F/\sigma)^{1/4}$, where $F = \int F_\nu d\nu$. The profile becomes a bit flatter in the vicinity of the black hole when $\dot{m} \gtrsim 30$ due to the photon-trapping effects. In particular, the slope becomes somewhat flatter than that predicted by the slim-disk model, $r^{-1/2}$, in the case of $\dot{m} = 100$. When $\dot{m} = 10$, in contrast, the profile is consistent with the standard-disk model, in which $T_{\rm eff} \propto r^{-3/4}$, except at

$r/r_{\rm g} \lesssim 7$, where boundary effects appear, since the photon-trapping effects are negligible. Here, it should be stressed that the flatter effective temperature means a reduction of the radiative flux at small radii, however, the local emergent spectrum is no longer a simple multi-color blackbody spectrum (discussed in the next subsection).
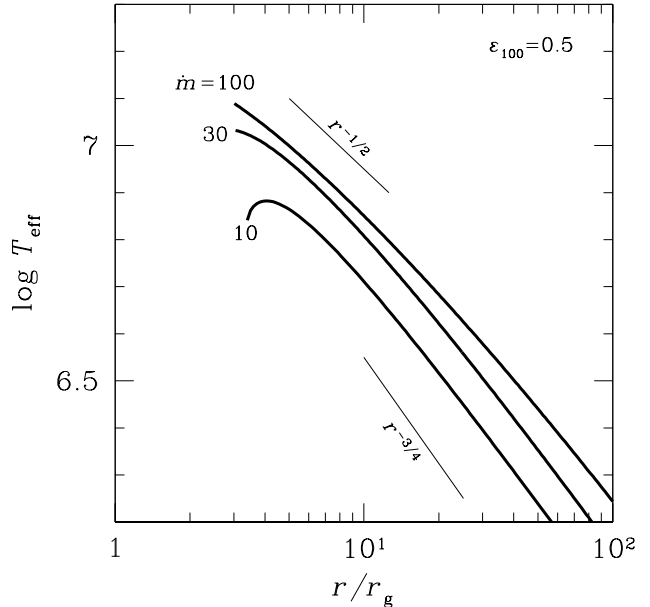

FIG. 2.— The effective temperature profiles for the case with $\varepsilon_{100} = 0.5$ for various $\dot{m}$; $\dot{m} = 10$, 30, and 100. Through the photon-trapping effects, the profile becomes flatter in the vicinity of the black hole as $\dot{m}$ increases beyond $\dot{m} \sim 30$. In particular, the profile for the case with $\dot{m} = 100$ is somewhat flatter than the prediction of the slim-disk model; i.e., $T_{\rm eff} \propto r^{-1/2}$.

3.3. *Spectral Energy Distribution*

We show the SED of the accretion flow with $\dot{m} = 10$ for $\varepsilon_{100} = 0.5$, 0.17, and 0.1 in Figure 3. For such a low $\dot{m}$, the photon-trapping effects do not appear yet, but the calculated SEDs grossly deviate from the SED predicted by the standard disk with the same $\dot{m}$, which is indicated by the dotted curve. It is found that the SED is shifted towards the higher-energy side as ε_{100} increases. This is explained by the transmission of high-energy photons generated near the equatorial plane, since for given $\dot{m}$ both of Σ and ρ decrease as ε_{100} increases, leading to a decrease of κ_ν, especially at high ν (note $\kappa_\nu \propto \rho^2$ and κ_ν decreases as ν increases). Then, the high-energy photons arising from deep inside the disk can pass through the disk body when ε_{100} is large. In the case of $\varepsilon_{100} = 0.5$ and 0.17, the frequency of the SED peak intensity (hereafter referred to as the peak frequency) is by about three times higher than that of the standard disk. This result might resolve the so-called 'too hot accretion disk problem' (Makishima et al. 2000). That is, the black-hole masses of some ULXs are inferred to be at least $\sim 100 M_\odot$, since their luminosities reach $\sim 10^{40} {\rm erg \ s^{-1}}$, while the source luminosities can not exceed the Eddington luminosity. Then, the standard-disk model predicts that the innermost disk temperatures of these objects should be $kT_{\rm in} < 1$ keV for $M \gtrsim 100 M_\odot$, however, the observed temperatures are much higher (1.1-1.8 keV). This is the 'too hot accretion disk problem.'
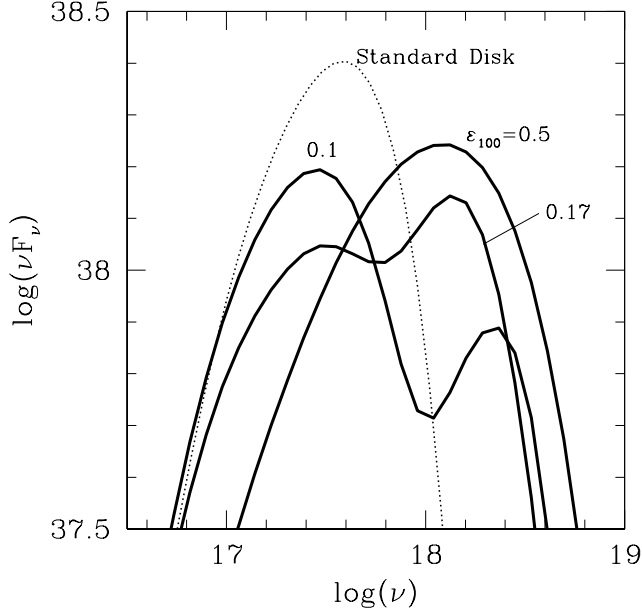
FIG. 3.— The spectral energy distribution (SED) of the accretion disk for $\dot{m} = 10$ and for $\varepsilon_{100} = 0.5$, 0.17, and 0.1. The dotted curve shows the SED predicted by the standard-disk model. The SED is shifted towards the higher-energy side with the increase of ε_{100}, since for large ε_{100}, Σ, ρ, and, hence, κ_ν are smaller so that the high-energy photons arising from deep inside the disk can easily pass through the disk body.

In our simulations, the spectral hardening of the emergent SED is caused by the transmission of the high-energy photons arising from deep inside the disk. The Comptonization is not taken into account in our simulations although it provides another important cause of the hardening. The hardening due to the Comptonization was demonstrated by Czerny & Elvis (1987) and Ross, Fabian, & Mineshige (1992) [see, however, Laor & Netzer (1989) for negative results]. Shimura & Takahara (1993) solved multi-frequency radiation transfer equations coupled with the hydrostatic balance and Comptonization, finding the spectral hardening factor of $\kappa \sim 1.7$.

When ε_{100} is small, say $\varepsilon_{100} = 0.1$, Σ and κ_ν are large, and, therefore, photons tend to be absorbed and re-emitted before reaching the disk surface. Thus, only low-energy photons which are generated near the disk surface can go out and thus the emergent SED becomes similar to that of the standard disk. However, since the absorption coefficient by the free-free absorption strongly depends on the frequency as ν^{-3}, a part of high-energy photons can directly pass through the disk, and a double peak appears (see the cases with $\varepsilon_{100} = 0.17$ and 0.1). Here, we should note that the higher-energy peak might disappear, if the metal absorption, which can be much more effective at high frequency, is included (discussed later).

The emergent SEDs in the case of $\dot{m} = 100$ is shown in Figure 4. As was mentioned above, the peak frequency tends to increase as ε_{100} increases due to the transmission of the high-energy photons. However, the SED in the case of $\varepsilon_{100} = 0.5$ is softer than other cases. This is caused by the photon-trapping effects. Since the higher-energy photons originate from deep inside the disk, they tend to be more effectively trapped in the flow than lower-energy ones. As a con-

sequence, the peak frequency of the emergent SED eventually turns to decrease as $\dot{m}$ further increases. That is, the photon trapping provides the counter effect to the transmission of the high-energy photons. Thus, the peak frequency of emergent photons starts to decrease when $\dot{m}$ exceeds some critical value [see equation (8)].
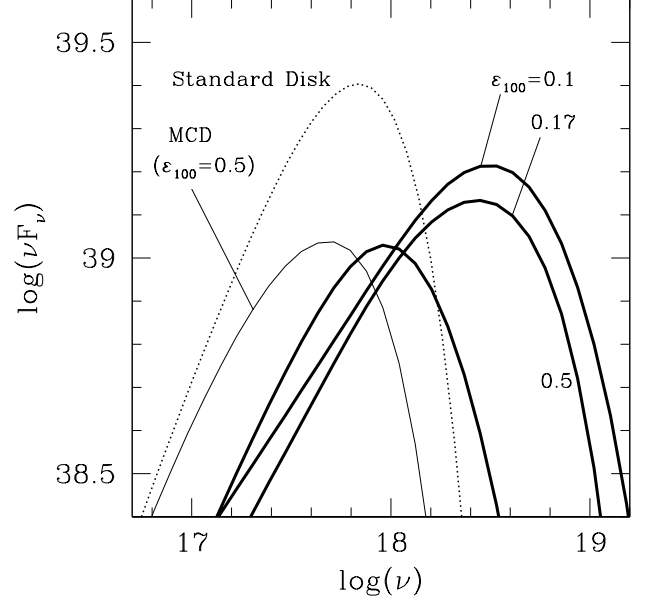
FIG. 4.— Same as Figure 3, but for $\dot{m} = 100$. The thin solid curve indicates the SED of the multi-color disk (MCD) model. The peak frequency of the SED becomes considerably low in the case of $\varepsilon_{100} = 0.5$ due to effective photon trapping. The MCD model does not correctly reproduce the actual SED.

In Figure 4, the thin solid curve is the SED of the multi-color disk (MCD) model for $\varepsilon_{100} = 0.5$, where the SED of the MCD model is calculated by the superposition of the blackbody spectra with various effective temperature, $B_\nu(T_{\rm eff})$ with $T_{\rm eff} \equiv (F/\sigma)^{1/4}$. As shown in this figure, the emergent SED is deviated from that of the MCD model. Therefore, not only the standard-disk model but also the MCD model can not successfully reproduce the actual SEDs in the supercritical accretion flow, and it is necessary to incorporate photon-trapping effects accurately when $\dot{m} \gtrsim 100$.

In Figure 5, we plot the variations of SED with changes in $\dot{m}$ for $\varepsilon_{100} = 0.17$ and 0.5. Symbols filled squares and circles indicate the locations of the SED peak. The peak frequency of the SED increases as the mass-accretion rate increases up to $\dot{m} = 30$ for both cases. When $\dot{m}$ is larger than 30, however, the peak frequency no longer increases, since the photon trapping works and tends to suppress the emergence of high-energy photons. In the case of $\varepsilon_{100} = 0.5$, in which the photon-trapping effects are more enhanced than the case of $\varepsilon_{100} = 0.17$, the peak frequency rather decreases with increase of the mass-accretion rate.
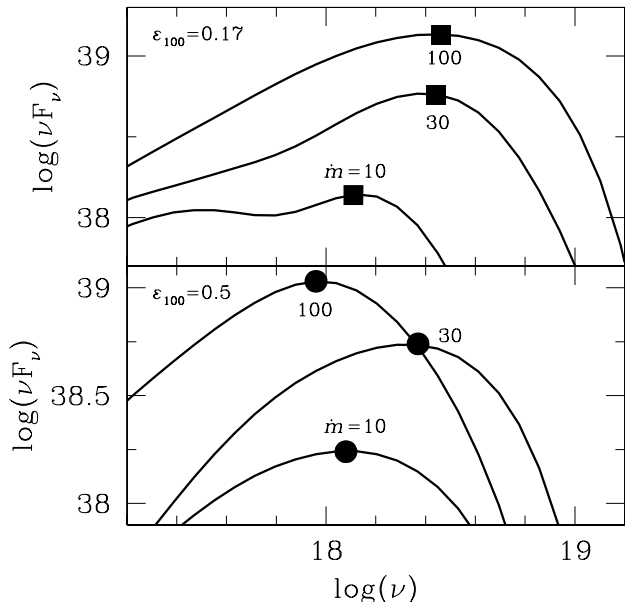
FIG. 5.— The SED for $\varepsilon_{100} = 0.17$ (upper panel) and 0.5 (lower panel) for different mass-accretion rates, $\dot{m} = 10$, 30, and 100. In contrast with the standard disk regime at $\dot{m} \leq 30$, in which the peak frequency increases with increasing $\dot{m}$, the peak frequency of the SED does not increase with an increase of mass-accretion rate when the photon trapping is effective ($\dot{m} \geq 30$). Rather, the peak frequency decreases as $\dot{m}$ increase, when $\varepsilon_{100} = 0.5$.

To sum up, the SED of the supercritical accretion flow shifts towards the higher-energy side owing to the transmission of high-energy photons as long as the photon-trapping effects are not appreciable. When $\dot{m}$ exceeds ~ 30, however, the photon-trapping effects become substantial if $\varepsilon_{100} \gtrsim 0.17$, and the peak frequency starts to decrease in spite of an increase of the mass-accretion rate.

3.4. Spectral fitting

3.4.1. X-ray H-R diagram

In the previous subsection, we overviewed the emergent SED in the supercritical accretion flow with careful considerations on the photon-trapping effects. Here, we fit the calculated spectra, following Watarai et al. (2000). In this fitting method, a simple temperature profile, $T_{\rm in}(r/r_{\rm in})^{-3/4}$ with $T_{\rm in}$ and $r_{\rm in}$ being fitting parameters, is employed for the model SED (Mitsuda et al. 1984). We adopt the photon energy range between 0.1keV and 5keV for the fitting, but we should keep in mind that the fitting results depend on the adopted energy range, in which the fitting is made. We plot the calculated $T_{\rm in}$ as a function of L in comparison with the observational data in the X-ray H-R diagram (see Figure 6).

As shown in Figure 6, $kT_{\rm in}$ increases as the mass-accretion rate increases for the case of $M = 10M_{\odot}$ and $\varepsilon_{100} = 0.17$ (filled squares). In the case of $\varepsilon_{100} = 0.5$ (filled circles), in contrast, the innermost temperature $T_{\rm in}$ decreases with increase of $\dot{m}$ when $\dot{m} > 30$. This is due to very efficient photon-trapping effects, by which the emergent SED shifts towards the lower-energy side, leading to a decrease in $kT_{\rm in}$. As was mentioned in the previous subsection, the photon-trapping effects are more conspicuous in the accretion flow with larger ε_{100}.
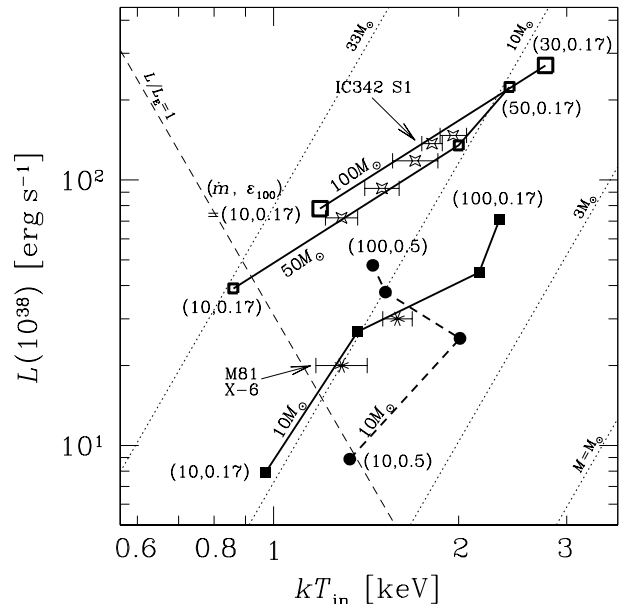

FIG. 6.— The predicted and observed trajectories of black-hole object with varying luminosity in the X-ray H-R diagram. The filled circles and filled squares indicate our numerical results for $\varepsilon_{100} = 0.5$ and 0.17, respectively, with different mass-accretion rates, $\dot{m} = 10$, 30, 50, and 100 from the bottom to the top. The small and big open squares represent the results for $\varepsilon_{100} = 0.17$, but the black-hole mass is $M = 50M_{\odot}$ and $100M_{\odot}$, respectively. A result of $\dot{m} = 100$ is not shown for $M = 50M_{\odot}$, and we plot only results of $\dot{m} = 10$ and 30 for $M = 100M_{\odot}$. The dotted lines correspond to the cases of the standard-disk model with different black-hole mass, $M = 1M_{\odot}$, $3M_{\odot}$, $10M_{\odot}$, and $33M_{\odot}$. According to the standard-disk model, the luminosity becomes the Eddington luminosity on the thin dashed line. The case of $(M, \varepsilon_{100}) = (10M_{\odot}, 0.17)$ nearly coincides with the observational results of M81 S-6. Moreover, the observed variation of IC 342 S1 can be reproduced by our model for $(M, \varepsilon_{100}) = (50 - 100M_{\odot}, 0.17)$.

In this figure, we found that the case of $\varepsilon_{100} = 0.17$ (filled squares) coincides most with the observational results of M81 S-6. The cases of $\varepsilon_{100} = 0.5$ (filled circles) does not reproduce the observed trend. Therefore, we can rule out the cases of $\varepsilon_{100} = 0.5$, that is, the photon-trapping effects should only moderately appear in the accretion flow of ULXs. This conclusion is supported by the fitting to the IC 342 S1 data, which is also well reproduced by the cases with $\varepsilon_{100} = 0.17$, if the black-hole mass is scaled up to $M = 50 - 100M_{\odot}$ (small and big open squares).

From the fitting to the IC 342 S1 data, we find that the black hole in IC 342 S1 is considerably massive; its mass is $50 - 100M_{\odot}$. Note that our estimation is by a factor of $1.7 - 3$ larger than the value $\sim 30M_{\odot}$ which Watarai, Mizuno, & Mineshige (2001) estimated based on the slim-disk model. Scatters of IC 342 S1 data in the H-R diagram is understood in term of the variation of the mass-accretion rate according to our model. If we adopt the standard-disk model, the black-hole mass should change to fit the observation which is, of course, unreasonable. Our model is certainly preferable.

3.4.2. Inner-edge radius and hardening factor

Next, we estimate the inner-edge radius, $R_{\rm in}$, by adopting equation (4) in Makishima et al. (2000) to our calculated SEDs. We assume that the hardening factor is

$\kappa = 1.7$ and the correction factor to $R_{\rm in}$, which is required to remove boundary effects is set to be $\xi = 0.42$. As shown in the upper panel of Figure 7, the resultant inner-edge radius depends on the parameter, ε_{100}, as well as the mass-accretion rate, $\dot{m}$; namely it depends on how important the photon-trapping effects are. The photon-trapping effects tend to increase the inner-edge radius and decrease of $T_{\rm in}$ because of suppression of emergence of high-energy photons. In the case of $\varepsilon_{100} = 0.5$, $R_{\rm in}$ drastically shifts from 40 km to 160 km as the mass-accretion rate increases from $\dot{m} = 30$ to 100 due to very efficient photon trapping. If $\varepsilon_{100} = 0.17$, conversely, the radius decreases with increase in the mass-accretion rate as long as $\dot{m} \lesssim 50$. At higher $\dot{m} > 50$, the radius slightly increases due to the mild photon-trapping effects.
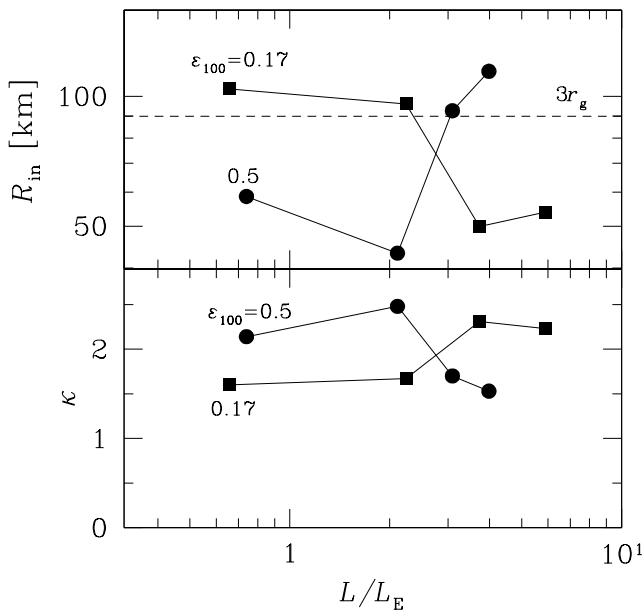

FIG. 7.— The inner-edge radius, $R_{\rm in}$ (upper panel) and the hardening factor, κ (lower panel) for the different mass-accretion rates, $\dot{m} = 10$, 30, 50, and 100, from the left to the right, respectively.

In the lower panel of Figure 7, we plot the hardening factor, κ, by employing equation (4) in Makishima et al. (2000). Here, we set $R_{\rm in} = 3r_{\rm g}$ and $\xi = 0.412$. It is clear in this figure that the hardening factor is reduced by the photon-trapping effects. In the case of $\varepsilon_{100} = 0.5$, κ decreases when $\dot{m}$ exceeds 30. If $\varepsilon_{100} = 0.17$, κ slightly increases for $\dot{m} < 50$, but it decreases at $\dot{m} > 50$ when photon-trapping effects are substantial.

4. DISCUSSION

4.1. Comparison with the Slim-disk Model

In some slim-disk approach, the emergent SED is assumed to be the superposition of blackbody spectra with different effective temperatures (Szuszkiewicz, Malkan, & Abramowicz 1996; Watarai et al. 2000). However, such a method is not successful in reproducing the actual SED as was shown in §3.3. Moreover, we found that the effective temperature profiles may deviate from the prediction of the slim-disk model, $r^{-1/2}$, at large $\dot{m}$ since the photon-trapping effects are not accurately treated in the slim-disk model (§3.2, see also Paper I).

Nevertheless the slim-disk model, as well as our model for the case of $\varepsilon_{100} = 0.17$, can reproduce the basic trend of the ULXs data in the X-ray H-R diagram (Watarai, Mizuno, & Mineshige 2001). However, we should stress that the physical reason to cause apparent decrease in $R_{\rm in}$ (or ratio of $L/T_{\rm eff}^4$) completely differ. In the slim-disk approach, the physical inner edge actually shifts and extends down to $\sim r_{\rm g}$ at high $\dot{m}$. The consequence is that the ULXs data can be fitted well with small $R_{\rm in}$. In our model, in contrast the disk inner edge is assumed not change, but the disk temperature increases apparently due to the transmission of the high-energy photons from deep inside. In realistic situations, both will work, but which is more important is not clear at the moment.

Finally, we indicate the important difference between the slim-disk model and our model. The black-hole mass of IC 342 S1 is estimated to be $\sim 30 M_\odot$ in the slim-disk approximation (Watarai, Mizuno, & Mineshige 2001), whereas it is considerably massive, $50 - 100 M_\odot$, in the present study. We need to remark on the limitations of the present model, however, since our model is essentially one-dimensional model and the flow structure is not properly solved. We need further studies (see below).

4.2. Future Work

Throughout the present study, we treated only the free-free absorption/emission and the Thomson scattering as physical interaction between gas and radiation. However, the Comptonization may play an important role on the emergent SED (Czerny & Elvis 1987; Ross, Fabian, & Mineshige 1992; Shimura & Takahara 1993). Then, the emergent spectra get even harder. If the corona exists above the disk, farther, the high-energy power-low photons will be generated by the inverse Compton scattering (Haardt & Maraschi 1991; Liu, Mineshige, & Ohsuga 2002). The emergent SED would be improved by simulations of radiation transfer which incorporates Comptonization, e.g., Monte Carlo simulations (Pozdnyakov, Sobol', & Sunyaev 1977).

The metal absorption may be effective at high frequency. Then, the high-energy photons generated deep inside the disk may be absorbed at a certain depth. If this is the case, the higher-energy peak may disappear and the peak of the emergent SED shift to lower-energy side. We expect that the emission lines by metals should be observed in the emergent SED. If the cross-section for the metal absorption is comparable to or more than that of the Thomson scattering, the photon trapping is drastically enhanced and the energy-conversion efficiency is more reduced. Then, such accretion flows will be observed as relatively dim and metal rich objects.

In this study, we adopted the plane-parallel approximation, which introduces error of $\sim (H/r)^2 \ll 1$. As future work, we need to solve full two-dimensional radiation transfer equations.

The convection which seems to occur when the disk is radiation pressure dominated (Shakura, Sunyaev, & Zilitinkevich 1978; Agol et al. 2001) would also reduce the photon-trapping effects. Since the high-energy photons trapped in the flow can be carried towards the disk surface by the convection, the high-energy photons emerge and the peak of the SED would be higher than that of

the expectation in our present study (see discussion in Mineshige et al. 2000).

The photon-trapping effects would be much reduced, if the gas density distribution is strongly patchy in the disk, since the photons can pass through the disk along the low-density regions. Begelman (2002) suggested that by such a effect the disk luminosity can exceed the Eddington luminosity. The details are not clear before multi-dimensional radiation-hydrodynamical (RHD) simulations are performed. Two-dimensional RHD simulations have been initiated by Eggum, Coroniti, & Katz (1987, 1988), and followed by Okuda, Fujita, & Sakashita (1997), Fujita & Okuda (1998), Kley & Lin (1999), Okuda & Fujita (2000), and Okuda (2002), though the radiation fields are treated in monochromatic form.

Finally, we employ the FLD approximation in the present work. Though this formulation well agrees with the exact solution both in the optically thick and thin regimes, it would be better to solve the radiation transfer equations without using the approximation. Especially, the FLD approximation might be invalid when the patchy structure forms inside the accretion flow, since the FLD approximation does not always give the exact solution at the regions of moderate optical thickness.

5. CONCLUSIONS

By solving the multi-frequency radiation transfer and the energy equations of gas as well as radiation, we have investigated the SED of the supercritical accretion flow with special attention on the photon-trapping effects. The present results are summarized as follows.

(1) For $L \lesssim 2L_{\rm E}$ ($\dot{m} \lesssim 30$), at which the photon trapping does not occur, the peak frequency of the resultant SED becomes, at maximum, three times higher than that expected by the standard-disk theory. This is a result of the transmission of the high-energy photons from deep inside because of smaller opacity for higher-energy radiation. This result might resolve the so-called 'too hot accretion disk problem' (Makishima et al. 2000).

(2) For $L \gtrsim 2L_{\rm E}$ ($\dot{m} \gtrsim 30$), the photon-trapping effects are substantial. Then, the high-energy photons are more efficiently trapped in the flow than the low-energy ones, since the former arise near the equatorial plane. Thus, the SED shifts towards the lower-energy side as $\dot{m}$ increases.

(3) By comparing with the observational data of ULXs in the X-ray H-R diagram, we found that the photon-trapping effects would only moderately appear in the accretion flow of ULXs. We can explain the observed time variations of IC 342 S1 on the X-ray H-R diagram in terms of $\dot{m}$ modulation. Its black-hole mass is estimated to be $M \sim 100 M_\odot$, which is greater than the previous estimate based on the slim-disk model, $M \sim 30 M_\odot$ (Watarai, Mizuno, & Mineshige 2001).

REFERENCES

Abramowicz, M. A., Czerny, B., Lasota, J. P., & Szuszkiewicz, E. 1988, ApJ, 332, 646
Agol, E., Krolik, J., Turner, N. J., & Stone, J. M. 2001, ApJ, 558, 543
Alme, M. L. & Wilson, J. R. 1976, ApJ, 210, 233
Begelman, M. C. 1978, MNRAS, 184, 53
Begelman, M. C. 2002, ApJ, 568, L97
Boller, T. 2000, NewAR, 44, 387
Colbert, E. J. M. & Mushotzky, R. F. 1999, ApJ, 519, 89
Collin, S. et al. 2002, A&A, 388, 771
Czerny, B. & Elvis, M. 1987, ApJ, 321, 305
Eggum, G. E., Coroniti, F. V., & Katz, J. I. 1987, ApJ, 323, 634
Eggum, G. E., Coroniti, F. V., & Katz, J. I. 1988, ApJ, 330, 142
Frank, J., King, A., & Raine, D. 1985, Accretion Power in Astrophysics (Cambridge: Cambridge Univ. Press)
Fujita, M. & Okuda, T. 1998, PASJ, 50 639
Fukue, J., Kato, S., & Matsumoto, R. 1985, PASJ, 37, 383
Haardt, F. & Maraschi, L. 1991, ApJ, 380, L51
Kato, S., Fukue, J., & Mineshige, S. 1998, Black-Hole Accretion Disks (Kyoto: Kyoto Univ. Press)
King, A. R., Frank, J., Kolb, U., & Ritter, H. 1997, ApJ, 482, 919
Kley, W. & Lin, D. N. C. 1999, ApJ, 518, 833
Kohri, K. & Mineshige, S. 2002, ApJ, 577, 311
Laor, A. & Netzer, H. 1989, MNRAS, 238, 897
Liu, B., Mineshige, S., & Ohsuga, K. 2003, ApJ, in press
Lynden-Bell, D. & Pringle, J. E. 1974, MNRAS, 168, 603
Makishima, K. et al. 2000, ApJ, 535, 632
Mihalas, D. & Klein, R. I. 1982, J. Comput. Phys., 46, 97
Mihalas, D. & Mihalas, B. W. 1984, Foundations of Radiation Hydrodynamics (Oxford: Oxford Univ. Press)
Mineshige, S., Kawaguchi, T., Takeuchi, M., & Hayashida, K. 2000, PASJ, 52, 499
Mitsuda, K. et al. 1984, PASJ, 36, 741
Mizuno, T., Ohnishi, T., Kubota, A., Makishima, K., & Tashiro, M. 1999, PASJ, 51, 663
Narayan, R., Piran, T., & Kumar, P. 2001, ApJ, 557, 949

Norman, C. & Scoville, N. 1988, ApJ, 332, 124
Ohsuga, K., Mineshige, S., Mori, M., Umemura, M. 2002, ApJ, 574, 315 (Paper I)
Ohsuga, K., Umemura, M., Fukue, J., & Mineshige, S. 1999, PASJ, 51, 345
Okada, K., Dotani, T., Makishima, K., Mitsuda, K., & Mihara, T. 1998, PASJ, 50, 25
Okuda, T., Fujita, M., & Sakashita, S. 1997, PASJ, 49, 679
Okuda, T. & Fujita, M. 2000, PASJ, 52, L5
Okuda, T. 2002, PASJ, 54, 253
Pozdnyakov, L. A., Sobol', I. M., & Sunyaev, R. A. 1977, Soviet Astron., 21, 708
Revnivtsev, M., Gilfanov, M., Churazov, E., & Sunyaev, R. 2002, A&A, 391, 1013
Ross, R. R., Fabian, A. C., & Mineshige, S. 1992, MNRAS, 258, 189
Rybicki, G. B. & Lightman, A. P. 1979, Radiative Processes in Astrophysics (New York: John Wiley & Sons, Inc.)
Shakura, N. I. & Sunyaev, R. A. 1973, A&A, 24, 337
Shakura, N. I., Sunyaev, R. A., & Zilitinkevich, S. S. 1978, A&A, 62, 179
Shimura, T. & Takahara, F. 1993, ApJ, 419, 78
Spruit, H. C. & Ritter, H. 1983, A&A, 124, 267
Stone, J. M., Mihalas, D., & Norman, M. L. 1992, ApJS, 80, 819
Szuszkiewicz, E., Malkan, M. A., & Abramowicz, M. A. 1996, ApJ, 458, 474
Turner, N. J. & Stone, J. M. 2001, ApJS, 135, 95
Umemura, M., Fukue, J., & Mineshige, S. 1998, MNRAS, 299, 1123
Wang, J. M., Szuszkiewicz, E., Lu, F. J., & Zhou, Y. Y. 1999, ApJ, 522, 839
Watarai, K., Fukue, J., Takeuchi, M., & Mineshige, S. 2000, PASJ, 52, 133
Watarai, K., Mizuno, T., & Mineshige, S. 2001, ApJ, 549, L77
Yamaoka, K., Ueda, Y., Inoue, H. 2001, in ASP Conf. Ser. 251, New Century of X-Ray Astronomy, ed. H. Inoue & H. Kunieda (San Francisco: ASP)